Supporting Information

Fluorination observed T_c increase of 110 K is challenging hydrogen-deuterium isotope effect

Yu-Ling Liu,[a] Si-Qi Lu,[b] Yuan-Yuan Tang,[a],* Xiao-Gang Chen,[b] Ji-Xing Gao,[b] Hao-Jie Li[b] and Ren-Gen Xiong[a,b],*

[a] Ordered Matter Science Research Center, Nanchang University, Nanchang 330031, People's Republic of China

[b] Jiangsu Key Laboratory for Science and Applications of Molecular Ferroelectrics, Southeast University, Nanjing 211189, People's Republic of China

Experimental section

Materials.

Triethylenediamine (Aladdin, 98%), Fluoromethyl iodide (Fluorio Pharmtech, 99%), Lead (II) iodide (Aladdin, 98%), *N,N*-dimethylformamide and tetrahydrofuran were used as received.

Synthesis.

The synthesis of *N*-FMedabco iodine salt is similar to the one for *N*-Medabco iodine salt.[1] We have made the synthesis a few changes for *N*-FMedabco iodine salt, which was successfully synthesized by adding 100 mmol fluoromethyl iodide dropwise to 100 mmol dabco tetrahydrofuran solution (200 ml) at room temperature, the mix of which was then stirred for 2 hrs and a large amount of white *N*-FMedabco iodine salt was filtered and dried in the 323 K oven. For the synthesis of **1**, 1 mmol of the two reagents (Lead (II) iodide and *N*-FMedabco iodine salt) were dissolved with 10 ml DMF respectively. Two cups of the solution are then mixed to produce a large amount of light-yellow precipitation. The above mixture was added with extra fresh 20 ml DMF solvent and heated at 373 K for 10 minutes. Then the mixture was cooled to room temperature before filtration to obtain a saturated solution. Yellowish rod-like crystals of **1** were reached by slow evaporation of the above saturated DMF solution at room temperature for one week.[2] Elemental analysis calcd (%) for $C_7H_{14}N_2FPbI_3$ (M_w: 733.11): C, 11.47; H, 1.92; N, 3.82; found: C, 11.78; H, 2.29; N, 3.67.

Methods.

PXRD measurements were taken on a Rigaku D/MAX 2000 PC X-ray diffraction instrument with Cu-Kα radiation (λ =1.5405 Å) in the 2θ range of 5-50° with a step size of 0.02°. The X-ray powder diffraction patterns of **1** and **2** at 293 K were fitted by the *Le-Bail* method using Rietica software. IR spectra of **1** in KBr pellets were recorded on a Shimadzu IR Prestige-21 instrument at room temperature. Thermogravimetric analyses (TGA) were carried out on a TA Q50 system with a heating rate of 10 K min^{-1} under a nitrogen atmosphere.

Differential scanning calorimeter (DSC) measurements for **1** and **2** were carried out on a PerkinElmer Diamond DSC instrument in the temperature range of 293 K-500 K with the same heating and cooling rate of 20 K min^{-1} under nitrogen atmosphere. The entropy change (ΔS) across the phase transition can be calculated from the enthalpy change (ΔH) in the differential scanning calorimetry (DSC) results. The ΔH for **1** and **2** during the transition at T_c are 12268.6 J mol^{-1} and 7601.6 J mol^{-1}. Based on the equation of $\Delta S \approx \dfrac{\Delta H}{T}$, the ΔS was estimated to be approximately 26.02 J (mol K)$^{-1}$ and 20.70 J (mol K)$^{-1}$ for **1** and **2**, respectively. According to the Boltzmann equation, $\Delta S = R \ln(N)$, where R is the gas constant and N is the ratio of the number of respective geometrically distinguishable orientations; the values of N for **1** and **2** are calculated as 26.03 and 12.05, respectively, suggesting that the molecule will show a very disordered state with approximate ellipsoid in high-temperature phase, which is comparable with the spherical molecules in plastic crystals.

Variable-temperature X-ray single crystal diffraction were performed on Rigaku Oxford Diffraction 2018 with Mo-Kα radiation ($\lambda = 0.71073$ Å) and the crystal data were collected at 293 K and 483 K, respectively. The Crystalclear software package (Rigaku, 2018) was used to process crystal data. The variable-temperature crystal structures were solved using a direct method, and the SHELXLTL software package (SHELXLTL-2014) was used for the refinement of crystal structures on F_2 using full-matrix least-squares refinement. The anisotropically of non-hydrogen atoms were refined for all reflections with I > 2σ(I) and the positions of the hydrogen atoms were generated geometrically. The DIAMOND software (Brandenburg and Putz, 2005) was used to draw asymmetric units and package views. For complex dielectric measurements, the polycrystalline samples were grinded into powder and then pressed into thin plates. The complex dielectric constants ($\varepsilon = \varepsilon'- i\varepsilon''$, where ε' is the real parts, and ε'' represents the imaginary parts) were measured by TongHui TH2828A instrument in the frequency range of 5 kHz to 1000 kHz with a temperature range of 293 K to 500 K. UV−vis diffuse-reflectance spectra measurements were performed at room temperature using a Shimadzu UV-2450 spectrophotometer mounted with ISR-2200 integrating sphere operating from 200 to 900 nm. BaSO$_4$ was used as a 100% reflectance reference.

Electronic structures calculation

The electronic structures calculations, including band structure and DOS were processed with the DFT method within the CASTEP code.[3,4] The initial structures were received from the Single-crystal structural diffraction at 293 K and were optimized before the electronic calculations. The Perdew–Burke–Ernzerhof in the generalized gradient approximation was employed to take the exchange and correlation effects into consideration.[5] The core-electrons interactions between the ionic cores and the electrons were described by the norm-conserving pseudopotential with the following valence electron configurations: Pb-5s^{2}5p^{6}5d^{10}6s^{2}6p^2, I-5s^{2}5p^5, C-2s^{2}2p^2, N-2s^{2}2p^3, F-2s^{2}2p^5 and H-1s^1.

Energy barrier calculation

The model structures of energy barrier calculations considering the effects from neighboring molecules of other cations and iodine anions were extracted from the X-ray crystallographically without further optimization. Energy barrier calculations were carried out by the DFT method with the Donald G. Truhlar hybrid M062-X functions in combination with suitable effective core potential (ECP) and basis set LANL08d used for the I atoms. The all-electron basis set 6-311G** was applied for H and F atoms, while all-electron basis set 6-31G* for C and N atoms.
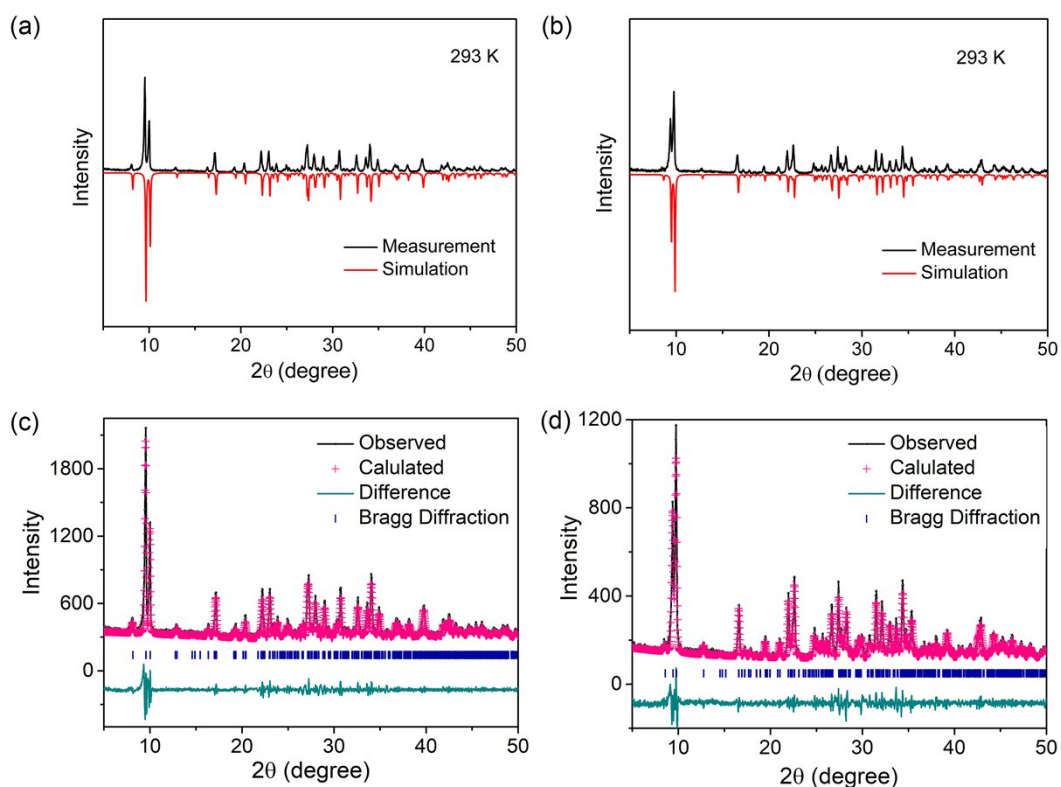
Fig. S1 Pattern of powder X-ray diffraction of **1** (a) and **2** (b) at 293 K and the Powder X-ray diffractograms refined by *Le-Bail* method of **1** (c) and **2** (d) at 293 K. The black line, pink symbol and the dark cyan continuous lines are the experimental, calculated and difference profiles, respectively. The vertical markers indicate the expected Bragg reflections. The corresponding refine parameters are Rp=13.30%, Rwp=18.41% and χ2=2.962 for **1** and Rp=12.59%, Rwp=16.78% and χ2=2.013 for **2**, respectively.
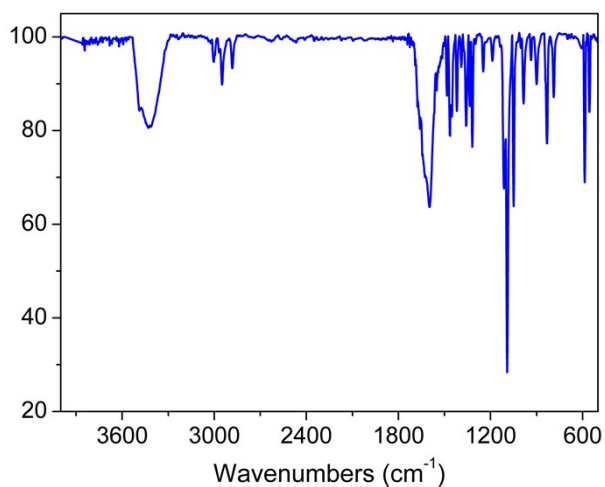
Fig. S2 IR spectra of **1**.

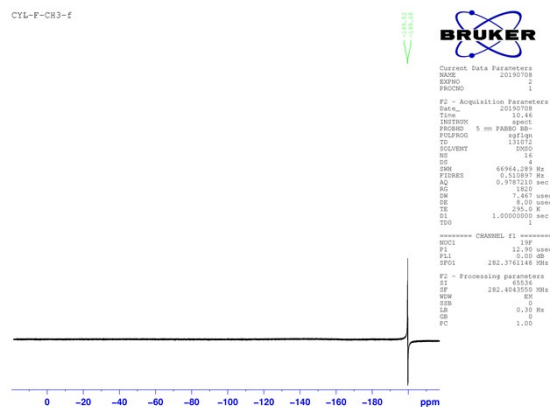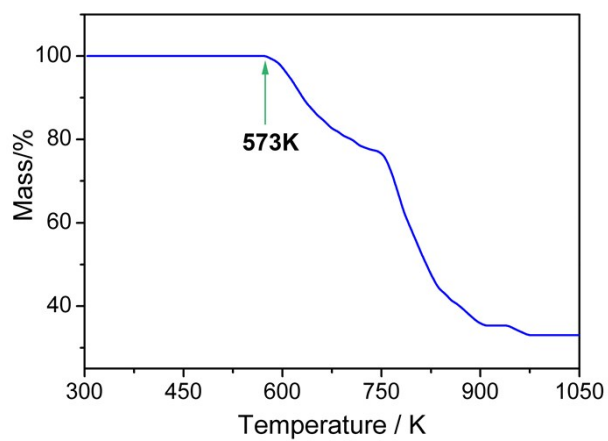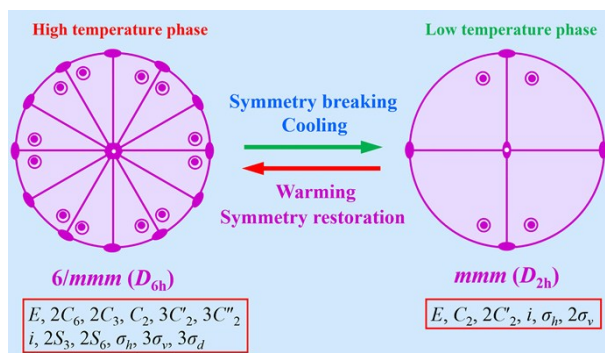**Fig. S3** The fluorine spectrum for **1**.
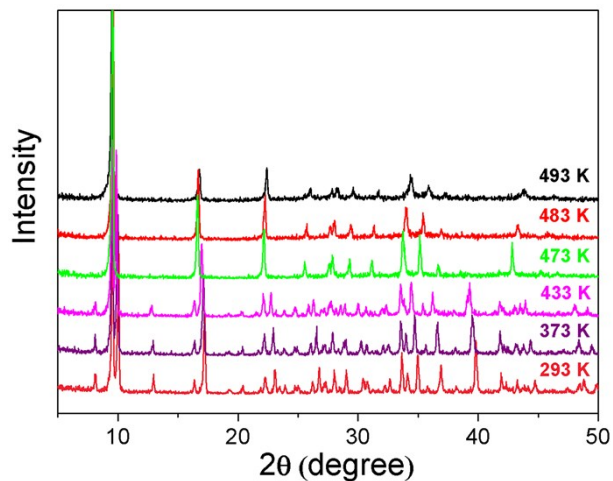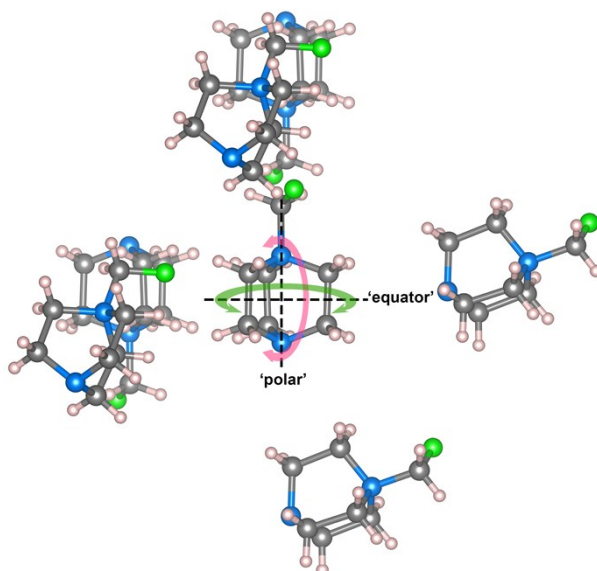

Fig. S4 TG analysis of **1**.

Fig. S5 Symmetry change in **1** of the LTP and HTP.

Fig. S6 Patterns of the powder X-rays diffraction (PXRD) measured for **1** at different temperatures.


Fig. S7 Two rotation models of *N*-FMedabco cations of **1** along 'equator' and 'polar' direction. The neighboring cations and iodine anions are included to explore the steric hindrance effects. Iodine atoms were omitted for clarity.
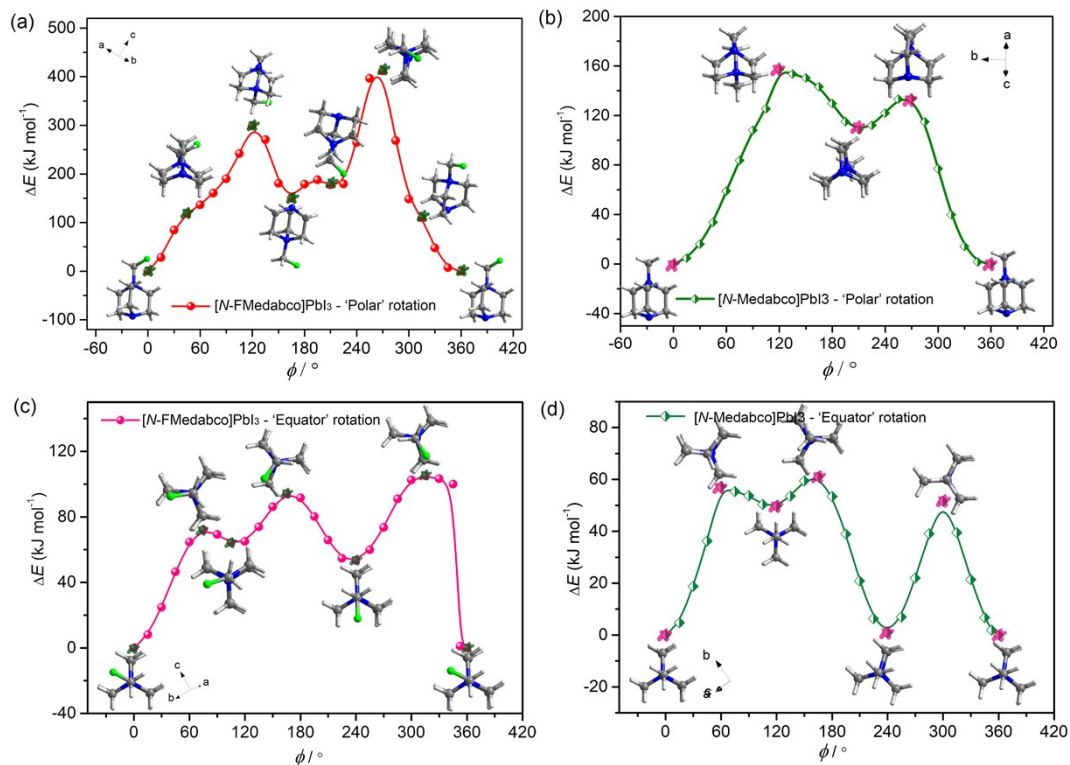
Fig. S8 The different displacements related to **1** and **2** correspond with the 'Equator' and 'Polar' rotation.

To understand the electronic semiconducting properties, the band structure and the partial density of states (PDOS) of **1** and **2** were carried out by employing the density functional theory (DFT). As presented in Fig. S9, the calculated results demonstrate that both **1** and **2** are direct bandgap semiconductors with the conduction band (CB) minimum and the valence band (VB) maximum localized at the G point and the band gap is 3.32 eV and 3.24 eV, respectively, larger than those of the experimental value of 2.97 eV (Fig. S10) and 2.92 eV.[2] The band structures are basically of the same shape except for the 0.08 eV band gap difference energy. As to the PDOS of **1** and **2**, the Pb-s/p and I-s/p states overlap apparently (Fig. S11) manifesting strong interactions between the Pb and I atoms. H-s, C-s/p and N-s/p states overlap with each other almost in the whole measured energy region, i.e., $-21 \sim -17$ eV, $-15 \sim -2.4$ eV, $-1 \sim -0.4$ eV, suggesting strong covalent bonds of C–N, C–H and N–H bonds in *N*-FMedabco and *N*-Medabco cations. Besides, F-s/p orbitals overlap intensively with C-s/p orbitals in the $-26 \sim -24$ eV and $-13.5 \sim -2.5$ eV region, illuminating the strong C–F bonding interactions in *N*-FMedabco cations. As displayed in Fig. S7, the maximum of VB bands is mainly derived from the nonbonding states of I-5p, and the minimum of CB bands originates from the unoccupied Pb-6p orbitals. So the band gap of the material relies on the inorganic part.
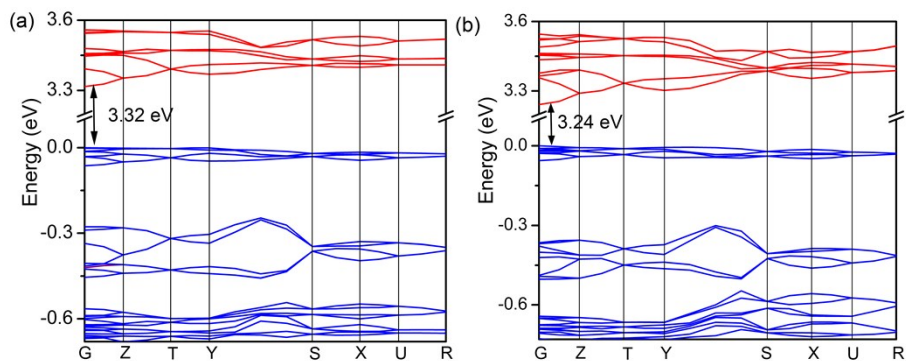
Fig. S9 Calculated band structure of **1** ([*N*-FMedabco]PbI₃) (a) and **2** ([*N*-Medabco]PbI₃) (b).
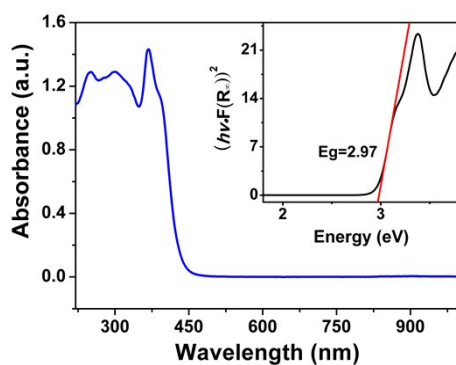
Fig. S10 UV-vis absorption spectrum of **1**. The inset shows the *Tauc* plot. The estimated band gap is 2.97V regarded as a direct band gap semiconductor.
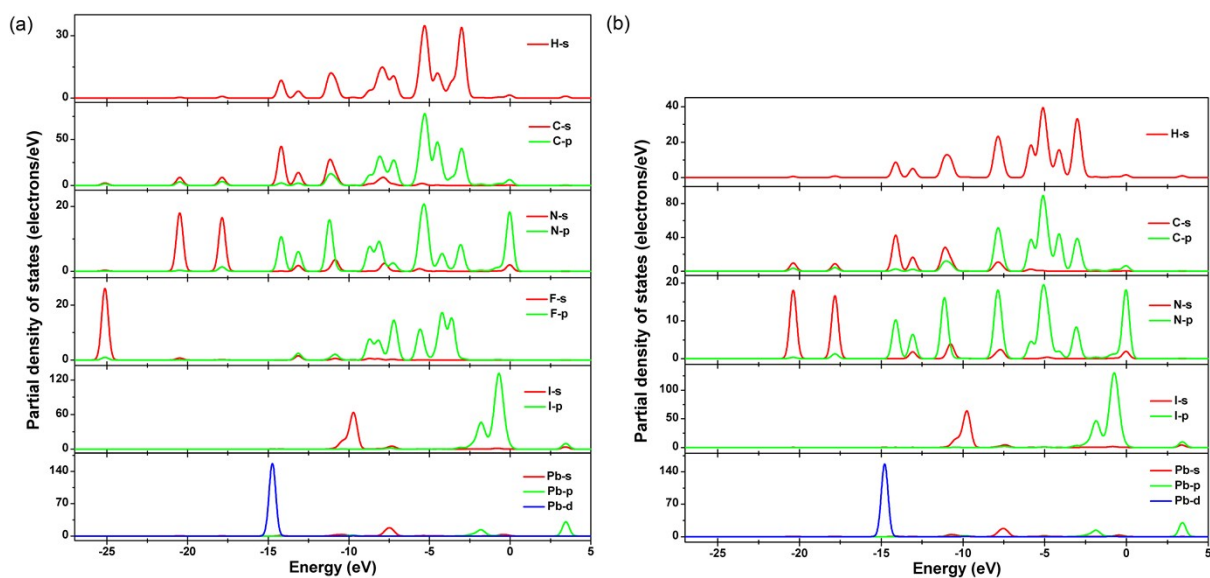
Fig. S11 PDOS of compound **1** and **2**.

Table S1. Crystal data and structure refinements for **1** at 293 K and 483 K.

Temperature/K	293	483
Crystal system	Orthorhombic	Hexagonal
Space group	*Pbca*	*P6₃/mmc*
a/Å	17.4558(5)	10.6336(7)
b/Å	8.0494(2)	10.6336
c/Å	21.4892(5)	8.1342(5)
α/deg	90	90
β/deg	90	120
γ/deg	90	90
Volume/Å^3	3019.4(1)	796.5(1)
Z	8	2
Density/g cm^{-3}	3.225	2.956
R_1 [$I>2\sigma(I)$]	0.0286	0.0406
wR_2 [$I>2\sigma(I)$]	0.0624	0.1292
GOF	1.069	1.064

Table S2. Bond lengths (Å) and bond angles (°) for **1**.

1 (298 K)	Å		°
Pb(1)−I(1)	3.1780(4)	I(2)−Pb(1)−I(1)	99.613(10)
Pb(1)−I(1)#1	3.2120(4)	I(2)−Pb(1)−I(1)#1	84.976(10)
Pb(1)−I(2)#2	3.3414(4)	I(1)−Pb(1)−I(1)#1	88.813(11)
Pb(1)−I(3)	3.2447(4)	I(2)−Pb(1)−I(3)#1	86.930(10)
Pb(1)−I(3)#1	3.2365(4)	I(1)−Pb(1)−I(3)#1	171.476(12)
C(1)−N(1)	1.494(6)	I(1)#1−Pb(1)−I(3)#1	86.311(10)
N(1)−C(4)	1.490(6)	I(2)−Pb(1)−I(3)	88.594(10)
N(1)−C(2)	1.497(6)	I(1)−Pb(1)−I(3)	86.740(10)
N(1)−C(6)	1.502(6)	I(3)#1−Pb(1)−I(3)	98.954(13)
F(1)−C(1)	1.346(6)	C(4)−N(1)−C(1)	110.7(4)
N(2)−C(5)	1.451(8)	C(1)−N(1)−C(2)	111.0(4)
N(2)−C(7)	1.463(7)	C(4)−N(1)−C(6)	108.5(4)
N(2)−C(3)	1.481(8)	C(1)−N(1)−C(6)	107.9(4)
C(4)−C(5)	1.523(7)	C(5)−N(2)−C(3)	109.2(5)
C(6)−C(7)	1.538(8)	F(1)−C(1)−N(1)	108.0(4)
C(2)−C(3)	1.516(8)	N(1)−C(2)−C(3)	109.1(4)

#1 −x+1/2, y+1/2, z; #2 −x+1/2, y−1/2, z

1 (483K)	Å		°
Pb(1)−I(1)#1	3.230(1)	I(1)#1−Pb(1)−I(1)#2	84.57(3)
Pb(1)−I(1)#2	3.230(1)	I(1)#1−Pb(1)−I(1)#3	95.43(3)
Pb(1)−I(1)#3	3.230(1)	I(1)#2−Pb(1)−I(1)#3	180.0
Pb(1)−I(1)#4	3.230(1)	I(1)#1−Pb(1)−I(1)#4	84.57(3)
Pb(1)−I(1)#5	3.230(1)	Pb(1)−I(1)−Pb(1)#6	78.04(4)
Pb(1)−I(1)	3.230(1)	N(1)−C(2)−H(2A)	109.5
N(1)−C(2)	1.38(3)	C(1)#7−C(1)−N(1)	109.0(7)
N(1)−C(1)	1.38(3)	C(1)−N(1)−C(2)	108.9(11)
N(1)−C(1)#7	1.38(3)	N(1)−C(1)−H(1A)	109.9
C(1)−C(1)#8	1.20(6)	C(1)#8−N(1)−C(2)	109.0(11)
N(1)−C(1)#9	1.38(3)		

#1 −x+2, −y+2, −z+1; #2 y, −x+y+1, −z+1; #3 −y+2, x−y+1, z; #4 x−y+1, x, −z+1; #5 −x+y+1, −x+2, z; #6 −x+2, −y+2, z−1/2; #7 −y+1, x−y, z; #8 −y+1, −x+1, −z+1/2; #9 −x+y+1, −x+1, z

Reference

1. D. V. Konarev, S. S. Khasanov, A. Otsuka, G. Saito, R. N. Lyubovskaya, *J. Am. Chem. Soc.*, 2006, **128**, 9292−9293.

2. C. Xue, Z. Y.Yao, J. Zhang, W. L. Liu, J. L. Liu, X. M. Ren, *Chem. Commun.*, 2018, **54**, 4321−4324.

3. M. D. Segall, Philip J. D. Lindan, M. J. Probert, C. J. Pickard, P. J. Hasnip, S. J. Clark and M. C. Payne1, *J. Phys. Condens. Matter*, 2002, **14**, 2717−2744.

4. V. Milman, B.Winkler, J. A.White, C. J. Pickard, M. C. Payne, E. V. Akhmatskaya, R. H. Nobes, *Int. J. Quantum Chem.* 2000, **77**, 895−910.

5. J. P. Perdew, K. Burke, M. Ernzerhof, *Phys. Rev. Lett.*, 1996, **77**, 3865−3868.